Received: 11 May 2023 | Revised: 20 September 2023 | Accepted: 27 November 2023

DOI: 10.1002/cyto.a.24814

ORIGINAL ARTICLE

MIFlowCyt

ISAC INTERNATIONAL SOCIETY FOR ADVANCEMENT OF CYTOMETRY

CYTOMETRY Journal of Quantitative Cell Science PART A

Human mesenchymal stem cells increase LLC metastasis and stimulate or decelerate tumor development depending on injection method and cell amount

Yurii V. Stepanov[1,2] | Iuliia Golovynska[1] | Galyna Ostrovska[3] | Larysa Pylyp[4] | Taisa Dovbynchuk[3] | Liudmyla I. Stepanova[3] | Oleksandr Gorbach[5] | Volodymyr Shablii[6,7] | Hao Xu[1] | Liudmyla V. Garmanchuk[3] | Tymish Y. Ohulchanskyy[1] | Junle Qu[1] | Galina I. Solyanik[2]

[1]Shenzhen Key Laboratory of Photonics and Biophotonics, College of Physics and Optoelectronic Engineering, Shenzhen University, Shenzhen, People's Republic of China

[2]Laboratory of Molecular and Cellular Mechanisms of Metastasis, R.E. Kavetsky Institute of Experimental Pathology, Oncology and Radiobiology, NAS of Ukraine, Kyiv, Ukraine

[3]Institute of Biology and Medicine, Taras Shevchenko National University of Kyiv, Kyiv, Ukraine

[4]Clinic of Reproductive Medicine "Nadiya", Kyiv, Ukraine

[5]Laboratory of Experimental Oncology, National Cancer Institute of Ukraine, Kyiv, Ukraine

[6]Institute of Molecular Biology and Genetics, NAS of Ukraine, Kyiv, Ukraine

[7]Institute of Cell Therapy, Kyiv, Ukraine

Correspondence
Iuliia Golovynska, Shenzhen Key Laboratory of Photonics and Biophotonics, College of Physics and Optoelectronic Engineering, Shenzhen University, Shenzhen 518060, People's Republic of China.
Email: iuliia@szu.edu.cn

Galina I. Solyanik, Laboratory of Molecular and Cellular Mechanisms of Metastasis, R.E. Kavetsky Institute of Experimental Pathology, Oncology and Radiobiology, NAS of Ukraine, Kyiv 03022, Ukraine.
Email: gsolyanik@gmail.com

Funding information
National Key R&D Program of China, Grant/Award Number: 2021YFF0502900; National Natural Science Foundation of China,

Abstract

Mesenchymal stem cells (MSCs) being injected into the body can stimulate or decelerate carcinogenesis. Here, the direction of influence of human placenta-derived MSCs (P-MSCs) on the Lewis lung carcinoma (LLC) tumor development and metastatic potential is investigated in C57BL/6 mice depending on the injection method. After intramuscular co-inoculation of LLC and P-MSCs (LLC + P-MSCs), the growth of primary tumor and angiogenesis are slowed down compared to the control LLC on the 15th day. This is explained by the fact of a decrease in the secretion of proangiogenic factors during in vitro co-cultivation of an equal amount of LLC and P-MSCs. When P-MSCs are intravenously (i.v.) injected in the mice with developing LLC (LLC + P-MSCs(i.v.)), the tumor growth and angiogenesis are stimulated on the 15th day. A highly activated secretion of proangiogenic factors by P-MSCs in a similar in vitro model can explain this. In both the models compared to the control on the 23rd day, there is no significant difference in the tumor growth, while angiogenesis remains correspondingly decelerated or stimulated. However, in both the models, the total volume and number of lung metastases constantly increase compared to the control: it is mainly due to small-size metastases for LLC + P-MSCs(i.v.) and larger ones for LLC + P-MSCs. The increase in the rate of LLC cell dissemination after the injection of P-MSCs is explained by the disordered polyploidy and chromosomal instability, leading to an increase in migration and invasion of cancer cells. After LLC + P-MSCs co-inoculation, the tumor cell karyotype has the most complex and heterogeneous chromosomal structure. These findings indicate a bidirectional effect of P-MSCs on the growth of LLC in the early periods after injection, depending on the injection method, and, correspondingly, the number of contacting cells. However, regardless of the injection method, P-MSCs are shown to increase LLC aggressiveness related to cancer-associated angiogenesis and metastasis activation in the long term.

Grant/Award Numbers: 62127819, 61835009; Shenzhen Key Laboratory of Photonics and Biophotonics, Grant/Award Number: ZDSYS20210623092006020; Shenzhen Science and Technology Program, Grant/Award Number: JCYJ20220818100202005; National Academy of Sciences of Ukraine, Grant/Award Number: 2.2.5.443

KEYWORDS

angiogenesis, cancer, human mesenchymal stem cells, Lewis lung carcinoma karyotype, tumor growth and metastasis

1 | INTRODUCTION

Mesenchymal stem cells (MSCs) are a type of multipotent cells with a high differentiation potential and the ability to self-renewal. They have an innate tropism to focal inflammation and malignancy, making them an important factor in oncogenesis research. The cancer-related effects of MSCs are predominantly associated with many bioactive molecules, which they synthesize and release into the environment. It is known that tumor secreted factors, similar to those secreted during inflammatory reactions, increase the recruitment of circulating MSCs into the tumor microenvironment [1–3]. MSCs can be isolated from a wide range of tissues: bone marrow (BM), adipose tissue, umbilical cord, umbilical cord blood, amniotic membrane and placenta, however, differences in their proliferation and behavior have been reported. Yet, the influence of different MSCs on morphological changes and angiogenesis in primary tumors, as well as on the dissemination processes of cancer cells is not fully understood. Literature data simultaneously describe two conflicting effects of MSCs on carcinogenesis: they can either promote [4–11] or decelerate [12–20] tumor growth in vitro and in vivo.

The MSC-induced stimulation of tumor growth is observed when different cancer cells mixed with BM-derived or tumor-associated MSCs transplanted subcutaneously exhibit an elevated capability of proliferation and angiogenesis in the tumor tissues and an increased metastatic ability [4, 5, 7, 8]. The stimulation after MSCs injection is observed due to their transformation into tumor-associated fibroblasts, immunosuppression, the stimulation of epithelial-mesenchymal transition of tumor stromal cells and malignancy of MSCs. MSCs escape immune recognition and inhibit immune responses of the major immune cells as well as inhibit lymphocyte proliferation [21–23]. This effect is based on the ability of MSCs to generate transforming growth factor-b1 (TGF-b1), hepatocyte growth factor, indoleamine 2,3-dioxygenase, inducible nitric oxide synthase, matrix metalloproteinase-2 and -9, prostaglandin E2 and sHLA-G5. The key event for the development of malignant neoplasms is the rapid growth of blood vessels inside tumor. MSCs activate hematopoietic and endothelial cells (EC) by releasing soluble factors such as angiopoietin-1, vascular endothelial growth factor (VEGF), platelet-derived growth factor, interleukin (IL) 8 and fibroblast growth factor-2/-7 [24, 25].

The MSC-induced deceleration of tumor growth is more frequently reported [12–20]. Animal transplantation studies show that the latent time of tumor formation is prolonged and the tumor size is smaller when mice are injected subcutaneously with human hepatoma cells and fetus dermal tissue-derived MSCs [13]. This effect is based on the ability of MSCs to suppress the expression of target proteins (namely, Bcl-2, cMyc, PCNA and survivin) of the Wnt signaling pathway. Intravenously (i.v.) injected MSCs can migrate to sites of tumorigenesis and potently slow down tumor growth via the inhibition of Akt activation [12]. Also, protein DKK-1 secreted by MSCs can suppress the Wnt signaling in cancer cells [12, 14]. In addition, BM-MSCs cause cell cycle arrest in the G0/G1 phase in hepatoma, lymphoma and insulinoma models [20]. Hence, MSCs and transformed cells have many common properties, in particular, self-renewal and differentiation regulated by similar signaling pathways, namely, Wnt, Notch, Shh and BMP.

Anti-cancer therapeutic potential of MSCs has been investigated in a small number of human clinical trials. Several of them are targeted against graft-versus-host diseases and to support the engraftment of hematopoietic SCs. Also, very few human clinical trials are in the oncology field to treat, in particular, gastrointestinal, lung or ovarian cancers [26–28]. So, MSCs possess high therapeutic potential [29], nevertheless, pathology such as malignant neoplasms requires special attention when using MSCs, since they are an important component of tumor microenvironment [1–3]. Moreover, the effect of MSCs may depend on such factors as their source, origin, subtype, injection method, and dose as well as carcinogenesis model. Hence, the described opposite effects of MSCs on cancers need further detailed research.

It is a common consideration currently that it is impossible to clearly define the relationship between the source, origin, and subtype of MSCs and cancer progression. For example, BM-MSCs show either stimulating [4, 5, 7–10] or decelerating effect [12, 17, 18, 20]. On the other hand, only Ryu et al [30] report the deceleration of MCF-7 cancer cell growth is increased with the amount of MSCs. Therefore, more detailed research is needed to be focused on their injection method and cell concentration, choosing a suitable MSC line. Among all MSC sources, the placental tissues are perinatal extraembryonic tissues and one of the most accessible sources of human MSCs, because of the least ethical restrictions, non-invasive methods of derivation, and a sufficient amount of cellular material. At the same time, placenta-derived MSCs (P-MSCs) exhibit some properties required for their use in cell therapy, in which they are superior to MSCs from other sources. Due to the expression of embryonic-specific markers, they are able to maintain an undifferentiated state and higher proliferative activity for a longer time and, moreover, they have a wider ability to differentiate. P-MSCs also demonstrate a faster growth kinetics and higher engraftment properties in recipient tissues as well as

exhibit high immunomodulatory and immunosuppressive properties, having a lower immunogenicity than adult BM-MSCs [31, 32]. In addition, P-MSCs are still a relatively understudied cell type for the impact on cancer progression.

The purpose of our current study is to investigate the influence of human P-MSCs on the growth rate, angiogenesis and metastatic potential of a tumor, depending on the administration method of P-MSCs together with cancer cells, that is, intramuscularly (i.m.) or i.v. injected. The model of primary transplantable murine Lewis lung carcinoma (LLC) investigated in C57BL/6 mice has been applied. The use of human MSCs in biomedical research and testing has an obvious advantage over those from laboratory animals, because there is no need to extrapolate the data obtained due to the presence of more relevant morphological, physiological and biochemical properties, including receptors. On the other hand, the LLC model is a known valid syngeneic tumor model employing mouse-derived cancer cells to investigate the development of tumor and metastasis.

2 | MATERIALS AND METHODS

2.1 | Animals

The animal studies were carried out using C57Bl/6 female mice, 10 weeks old, weighing 18–21 g. All the animal experiments were performed at the Institute of Biology and Medicine at Taras Shevchenko National University of Kyiv (IBM-TSNUK) in Ukraine and carried out in accordance with "Guide for the care and use of laboratory animals" and the experimental protocol approved by the Bioethics Committee of Animal Experiments in IBM-TSNUK. The mice were maintained in collective cages under standard controlled conditions on a 12 h light/dark cycle and fed standard rodent chow and water.

2.2 | Human P-MSCs and LLC cells

Term placentas were collected 39–41 weeks of gestation in the Kyiv city maternity hospital #3. All donors provided written informed consent for the sourcing and the usage of their placentas for the approved study. All details about the obtaining of MSCs and LLC cells are in Methods and Figures S1 and S2, Supplementary Materials.

2.3 | Flow cytometry

Cell suspension with P-MSCs was washed twice with cold Dulbecco's phosphate buffered saline DPBS (Sigma, USA). Samples were incubated for 30 min at +4°C and washed with cold DPBS for 10 min at 300 × g. Cells at 5×10^5 cells/mL in PBS were resuspend and added into cytometry tubes. Antibody cocktail consists of the primary anti-CD90 FITC, -CD105 PerCP-Cy5.5, -CD73 PE, -CD34 APC, and -CD45 APC-Cy7 were added to the samples at appropriate concentrations (Table S1, Supplementary Materials). The samples were incubated for 30 min at +4°C and washed with cold DPBS for 10 min at 300 × g. To each samples a 500 µL of DPBS were added and stored in a dark place at 4–8°C until analyzed on flow cytometer.

The samples were measured on a BD FACSAria III cell sorter (Becton Dickinson, USA) and analyzed using the BD FACSDiva v9.0 software. To adjust the compensation settings of fluorochromes, additional control samples were used: unstained control, single stained and fluorescence minus one control.

2.4 | Statistical analysis

Control and sample measurements were subjected to statistical analysis using two-way ANOVA with Tukey's post hoc test, using the OriginLab software. The results were expressed as the means ± SE; significance was set at $p < 0.05$.

3 | RESULTS

3.1 | Influence of P-MSCs on LLC tumor development in C57BL/6 mice

Figure 1 represents the characterization of the used human P-MSCs. P-MSCs are positive for CD90, CD105 and CD73 surface parkers, which is typical for MSC. Moreover, P-MSCs are negative for hematopoietic stem cell marker CD34 and pan leukocyte marker CD45 [31]. Our resulting P-MSCs must have a phenotype $CD90^+CD105^+CD73^+CD45^-CD34^-$. The viable MSCs were gated from a cultured cell population, therefore, gated cells with a high FSC rate and a low SSC rate.

To investigate the influence of P-MSCs on the tumor growth, angiogenesis, and metastasis, the next in vivo screening protocol was designed. All C57BL/6 mice were randomly divided into six experimental groups; the first three main groups were of 10 animals in each (the timeline of main groups is drawn in Figure S3). The mice of the 1st group were i.m. injected with 5×10^5 of LLC cells in 100 µL of saline into the right thigh muscles (the LLC group). The 2nd group mice were simultaneously i.m. injected with 5×10^5 of LLC cells and 5×10^5 of P-MSCs in 100 µL of saline into the right thigh muscles (the LLC + P-MSCs group). The 3rd group mice were i.m. inoculated with 5×10^5 of LLC cells in 100 µL of saline into the right thigh muscles, then 5×10^5 of P-MSCs were i.v. injected into the tail vein on the 7th day of LLC development (the LLC + P-MSCs(i.v.) group). The main studies were carried out on the 10th, 15th and 23rd day of LLC development. The resulted alterations of tumor growth and metastatic potential in the experimented mice with LLC + P-MSCs and LLC + P-MSCs(i.v.) were compared to the control mice with pristine LLC.

The 4th–6th groups are of 5 animals in each. The 4th group included control intact animals. The 5th group mice were i.m. inoculated with 5×10^5 of P-MSCs in 100 µL of saline into the right thigh muscles. The 6th group mice were i.v. injected with 5×10^5 of P-MSCs in 100 µL of saline into the tail vein. The mice of

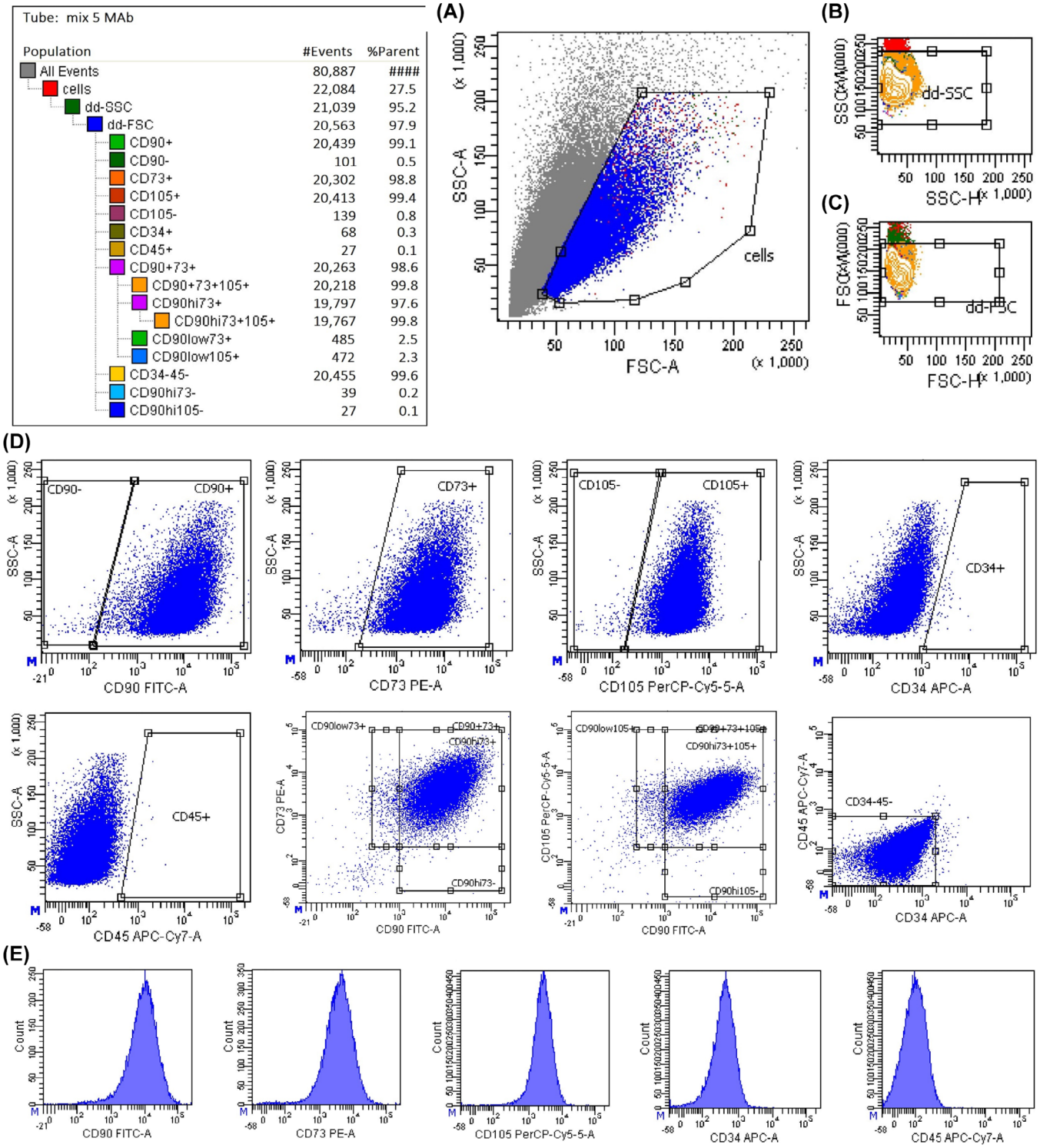

FIGURE 1 Immunophenotype of P-MSC by flow cytometry. (A) Cell distribution using the SSC-A and FSC-A parameters. (B) and (C) doublet discrimination using SSC and FSC to exclude the doublets and clumps from gate "cells" on the dot plot A. (D) The dot plots of the surface marker expression by P-MSC, such as CD90, CD73, CD105, CD45, and CD34. (E) The histogram plots of the P-MSC marker expression. The FACS data showed a high expression of P-MSC specific surface markers (CD90, CD73, and CD105) and the absence of CD45 and CD34 markers. Mesodermal differentiation with the vimentin expression presented in the Supplementary Materials (Figure S1). [Color figure can be viewed at wileyonlinelibrary.com]

these three groups were healthy without observed pathologies of the body tissues (the observation of pathologies in vivo is described in Supplementary Materials).

Figure 2 shows the influence of P-MSCs on LLC in the LLC + P-MSCs and LLC + P-MSCs(i.v.) tumor models. Figure 2A presents the photographs of extracted LLC tumors. The average tumor volume of

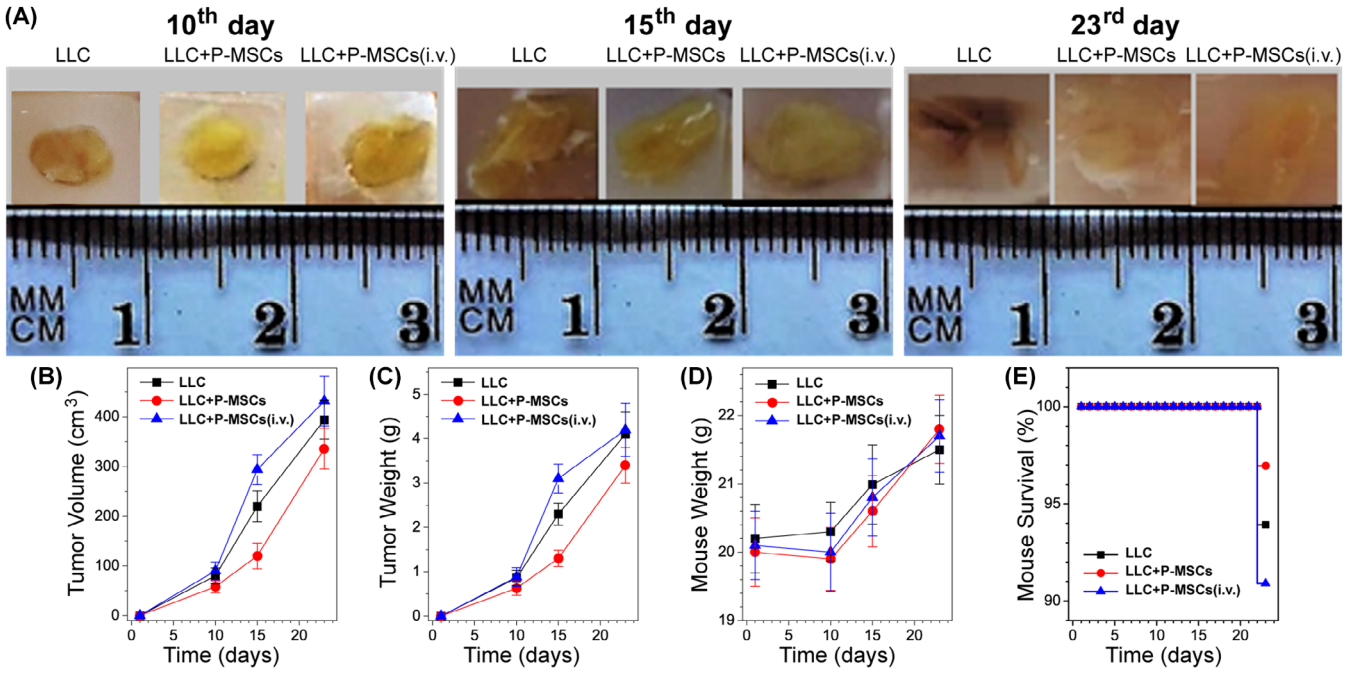

FIGURE 2 Oppositely directed influence of P-MSCs on LLC tumor development in C57BL/6 mice. (A) The representative images of the paraffin-embedded tissue blocks on the 10th, 15th, and 23rd day in the group LLC, LLC + P-MSCs and LLC + P-MSCs(i.v.). (B) Tumor volume, (C) tumor weight, (D) mouse body weight, and (E) survival in dynamics in the groups ($n = 10$) are shown as the mean ± SE from each group, $p < 0.05$ for data with a statistically significant difference (two-way ANOVA test). [Color figure can be viewed at wileyonlinelibrary.com]

all studied mice was ~80, 210, and 390 cm^3 on the 10th, 15th, and 23rd day (Figure 2B). The tumor weight was ~0.8, 2.3, and 4.1 g on the 10th, 15th, and 23rd day (Figure 2C). The main result is that, on the 15th day, the tumor volume and weight of LLC + P-MSCs were substantially lowered by ~1.8 times (118 cm^3 and 1.3 g); on the contrary, those of LLC + P-MSCs(i.v.) were increased by 1.4 times (293 cm^3 and 3.1 g) compared to the control pristine LLC tumor. Whereas, on the 10th and 23rd day, the tumor parameters in the groups did not statistically differ. The body weight of animals did not differ in all groups during all the experiment period and was ~20, 21, and 21.5 g on the 10th, 15th, and 23rd day (Figure 2D). Over 23 days, the animal survival was slightly enhanced (97%) in case of LLC + P-MSCs and decreased (91%) in mice with LLC + P-MSCs(i.v.) compared to 94% in the control LLC group (Figure 2E).

3.2 | Histological analysis of the P-MSC influence on LLC growth and angiogenesis

Figure 3 presents histopathology of growth and angiogenesis of transplanted LLC tumor during independent development. An intact muscle tissue has a typical histological structure with striated muscle fibers having numerous peripherally arranged nuclei (Figures 3A and S4). On the 5th day of LLC development, LLC cells infiltrate muscle fibers (Figure 3B), and primary tumor nodes start gradually form (Figure 3C). Zoomed images and detailed descriptions are presented in Figures S4, S5, S6, S8, and S10, Supplementary Materials.

On the 10th day, the main tumor node is characterized by the presence of honeycomb structures along the periphery, originating from muscle fibers on which the primary tumor nodes begin to form (Figure S7a). In the formed tumor, the cells are anaplastic and polymorphic, with sizes ranging 10–17 μm. They are mostly round-like but also irregularly, spindle and club shaped (Figure S7a). Large nuclei are observed (a nuclear-to-cytoplasmic ratio of 0.6–0.7) with 5–7 mitotic figures (Figure S7b). A noticeable vascularization occurs. The tumor provascular structures are localized closer to the node center, the sprouting of which is ~50% of the area (Figures 3D(i) and 5B), while vessels are found in a scant quantity in the tumor periphery (Figure 3D(ii)). EC are not observed (Figure 3D), indicating that vascularization occurs not due to the expansion of the vascular network already existing in the surrounding tissues but mainly due to the formation of new vessel-like structures (VLSs). The VLSs total area in the central part of the node is 36 μm^2 per 1000 μm^2 area (Figure S19b).

LLC + P-MSCs on the 10th day have a slightly different histopathological view, while their total histological morphology is similar to that of pristine LLC tumor: a pronounced cellular/nuclear polymorphism (Figures 4A(i) and S13a) and honeycomb structures (Figure S13b). The difference is in a significantly lower level of angiogenesis in the tumor node (the area of VLSs is 5 μm^2). Reliably determined VLSs are mostly absent (Figures 4A and S19b); individual small VLSs with sole erythrocytes are found only in a few areas of the periphery (Figures 4A(ii) and S13c). Zoomed images and detailed descriptions are presented in Figures S12, S14, S15, S16, S17, and

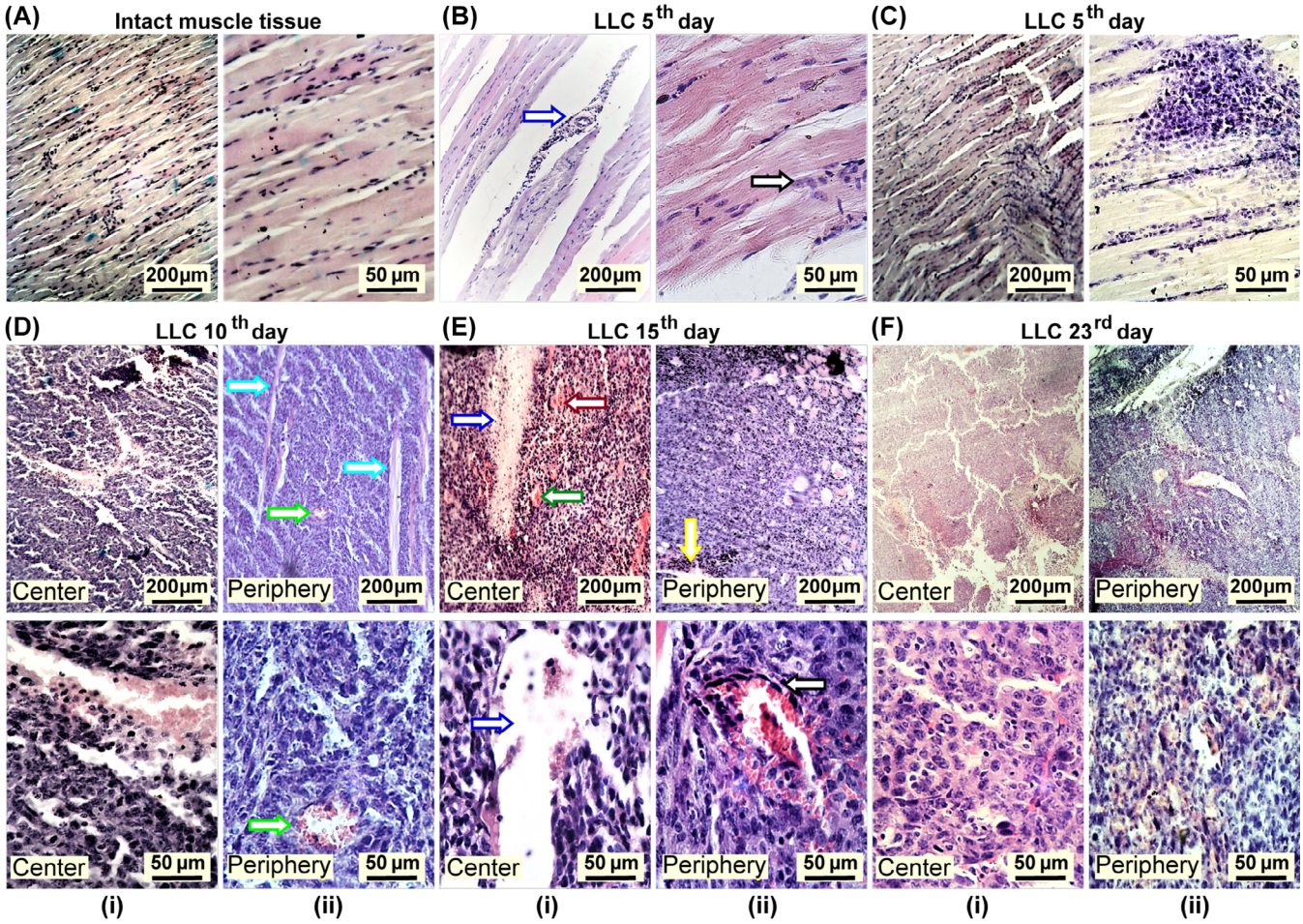

FIGURE 3 Histopathology of growth and angiogenesis of transplanted LLC tumor during independent development. Microscope images showing the initial stages of the tumor formation in a muscle tissue: (A) An intact muscle tissue; (B) LLC on the 5th day with the tumor cell aggregation around an arteriole (blue arrow) and the diffuse distribution of proliferating LLC cells along the bundles of muscle fibers (black arrow), (C) a formed tumor node; (D) LLC on the 10th day with (i) provascular formations in the node center and (ii) cellular and nuclear polymorphism at the tumor periphery (green arrow) and muscle fibers (blue arrow); (E) LLC on the 15th day with (i) multiple provascular formations in the center adjacent to the necrosis zone (blue arrow) and (ii) absent differentiated vessels in the periphery; (F) LLC on the 23rd day with (i) reserved tumor areas in the central part with decaying newly formed microvessels and (ii) a spread of foci of necrotic decay in the periphery. Zoomed images and detailed descriptions are presented in Figures S4, S5, S6, S8, and S10, Supplementary Materials. [Color figure can be viewed at wileyonlinelibrary.com]

S18, Supplementary Materials. So, the blood supply to the node obviously occurs via pre-existing vessels in the surrounding tissues.

On the 10th day in LLC + P-MSCs(i.v.), a noticeable vascularization occurs in the central part (Figure 4D(i)). Newly formed irregular or slit-shaped vessels are visible while they are without typical vascular walls, however, single-layer limiting walls resembling capillary endothelium are formed of LLC cells. In such VLSs, erythrocyte aggregation with the "sludge" phenomenon can be observed, as well as migrating tumor cells. The area of VLSs of 39 μm^2 does not significantly differ from LLC (Figure S19b). In the peripheral part, there are practically no vessels (Figure 4D(ii)). In the formed tumor nodes, a moderate cellular polymorphism is observed; the cells are anaplastic, polymorphic, mostly round-like, less fusiform, club-shaped and with large nuclei (Figure 4D).

In LLC on the 15th day, the central necrosis zones appear to be 7% of the tumor area (Figure S19a) and the vasculogenic mimicry is significantly increased: the area of VLSs is 48 μm^2 (Figures 3E(i) and S19b). Near the necrotic zones, there are many foci with extravasated erythrocyte masses due to vascular destructions. The tumor cells of the node are characterized by cellular/nuclear polymorphism: variations in size and shape as well as nuclear vacuolization and bizarre mitosis. In the periphery, there are very few vessels or VLSs and, in single cases, endothelial-like structures begin to form (Figure 3E(ii)). There are vessels with vascular walls differentiated by the type of arterioles and lined by flattened ECs (Figure S9a) and veins at the tumor node edge and subcutaneous adipose tissue (Figure S9b).

In LLC + P-MSCs on the 15th day, the area of necrosis is 12%, so, ~1.8 times larger than in pristine LLC (Figures 4B(i) and S19a). Neoangiogenesis becomes pronounced (the area of VLSs is 8 μm^2), though, with the rate lagging behind that in pristine LCC (Figure S19b). There are many provascular structures clean of aggregated erythrocytes. The cells of the node have a low degree of

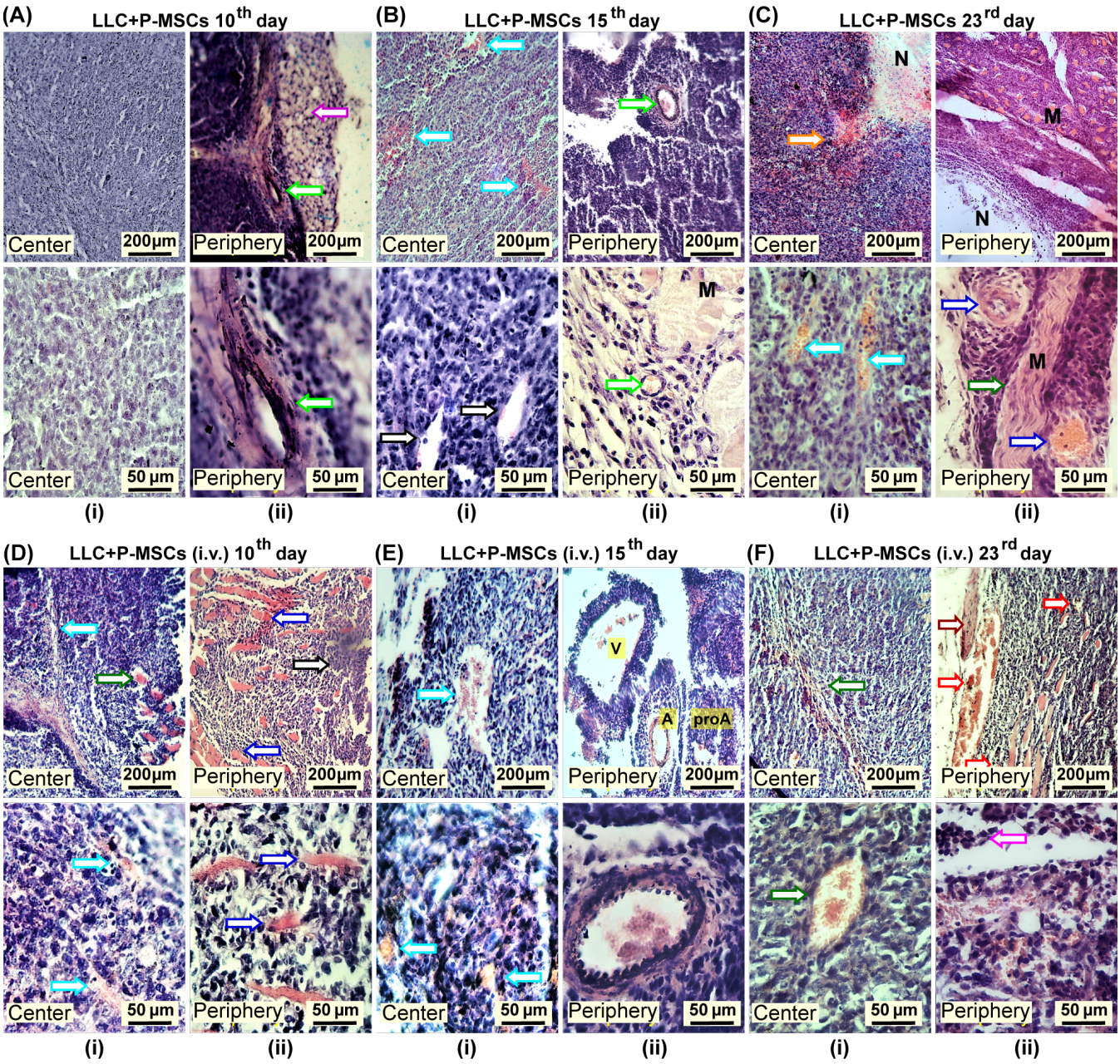

FIGURE 4 Histopathology of growth and angiogenesis in the LLC + P-MSCs and LLC + P-MSCs(i.v.) tumor models. (A) LLC + P-MSCs on the 10th day: (i) absent angiogenesis in the tumor center; (ii) pre-existing differentiated vessels at the edge of the tumor node (green arrow) and subcutaneous adipose tissues (violate arrow). (B) LLC + P-MSCs on the 15th day: (i) provascular formations in the central part of the tumor node with absent necrosis (blue arrow); (ii) differentiated vessels at the tumor node edge (green arrow). (C) LLC + P-MSCs on the 23th day: (i) erythrocyte hemorrhages in the area adjacent to necrosis (orange arrow), tumor nodes, newly formed provascular formations with a preserved structure and tumor cells migrating into them (blue arrow); (ii) a complete necrotic (N) disintegration of the main tumor bulk in the periphery and a relatively preserved part adjacent to muscle fibers (M). (D) LLC + P-MSCs(i.v.) on the 10th day: (i) initial provascular structures with erythrocytes in the tumor (blue arrow) and muscle fibers (green arrow); (ii) no pronounced signs of angiogenesis and maintaining contact of the growing tumor node with muscle tissues. (E) LLC + P-MSCs(i.v.) on the 15th day: (i) provascular structures with an erythrocyte mass actively formed in the tumor center (blue arrows); (ii) numerous differentiated vessels in the periphery (V – large vein, A – arteriole, proA – an intratumoral provascular structure). (F) LLC + P-MSCs(i.v.) on the 23rd day: (i) an intense neoangiogenesis in the tumor center (green arrows); (ii) in the tumor node periphery, a large vein and capillaries sprouting from the surrounding tissues filled with erythrocytes and migrating tumor cells (red arrows), preserved muscles (burgundy arrow), destruction of the existing vascular structures with irregular walls, extravasation of erythrocytes, secondary tumor nodes (tumor embolus, violet arrow) in the lumen of the tumor vessel. Zoomed images and detailed descriptions are presented in Figures S12, S14, S15, S16, S17, and S18, Supplementary Materials. [Color figure can be viewed at wileyonlinelibrary.com]

differentiation with many manifestations of cellular/nuclear polymorphism: significant variations in size and shape, hyperchromic nuclei, nuclear and cytoplasmic vacuolization, early pyknosis and bizarre mitosis. In the node periphery, single vessels with differentiated endothelial walls are observed (Figure 4B(ii)). The difference of angiogenesis in the presence of P-MSCs is a precise formation of provascular structures, herewith, vasculogenic mimicry is observed. Even in the presence of rouleaux formations, LLC + P-MSCs practically has no diapedetic (extravasal) erythrocyte masses (Figure 4B).

In LLC + P-MSCs(i.v.) on the 15th day, the area of necrosis is 14%, so, 2.2 times larger than in LLC (Figure S19a). The provascular structures are actively formed in its central part (the area of VLSs is 69 μm^2), more actively than in LLC, and separate large provascular structures with irregularly shaped lumens are observed (Figure 4E(i)). In the area adjacent to the forming necrosis, VLSs are mainly small. In the periphery, it can be noted that new VLSs are formed in the tumor; however, the vessels branching from the vascular network of surrounding tissues are practically absent. The tumor periphery actively uses such remodeled vessels to better support the tumor growth. On the other hand, the tumor VLSs are less developed (Figure S19b). The rate of cellular/nuclear polymorphism is increased (Figure 4E(ii)).

On the 23rd day, LLC tumor enters a state of decay characterized by 63% of necrosis area. The bulk of the tumor nodes becomes necrotic and fragmented (Figure 3F). In the tumor center, both extensive necrotic (Figure S19a) and preserved tumor areas with newly formed vessels are present with the area of VLSs of 54 μm^2 (Figures 3F(i) and S19b). In the node periphery adjacent to the necrosis areas, the destruction of vascular structures and the extensive areas of diapedesis hemorrhages are observed (Figures 3F(ii) and S11a,b). The preserved VLSs become larger (Figure S11c) and possess pronounced cellular polymorphism (Figure S11d).

On the 23rd day in LLC + P-MSCs, the necrotic area is insignificantly increased up to 78% (Figures 4C and S19a). In the necrotic area, the sites with diapedesis of erythrocytes appear (Figure 4C(i)), evidencing the destruction of vascular structures, with the area of VLSs of 28 μm^2 (Figure S19b). In the tumor peripheral preserved areas, vessels mainly have a pronounced tubular structure with endothelium-like walls (Figure 4C(ii)). But, the total number of VLSs is still significantly smaller than in pristine LLC. The preserved tumor areas also have pronounced cellular polymorphism (Figure 4C(i)). In the periphery, there are areas with small cell clusters associated with the surrounding muscle fibers and vessels (or adjacent to them) (Figure 4C(ii)).

On the 23rd day in LLC + P-MSCs(i.v.), the necrotic area is insignificantly increased up to 79% (Figures 4F and S19a), however, a much greater number of differentiated vessels (the area of VLSs is 78 μm^2) is observed in the central part (Figures 4F(i) and S19b) than in LLC (Figure 3F(i)). Neoangiogenesis is still observed (Figure 4F(i)). Many similar vascular structures with denser endothelium-like walls are partially destroyed. The numerous cells with karyorrhexis and karyolysis are seen. Surviving tumor cells have signs of proliferative activity: nucleus, nucleolus, lots of chromatin and mitotic figures are preserved (Figure 4F(i)). In the periphery, vessels are actively used (Figures 4F(ii) and S19b). The vessels of tissue and tumor are probably used for vascular migration of the tumor cells. The necrotic processes intensify, while the tumor tissue and vascular structures are destroyed, being accompanied by a massive release of erythrocytes into the intercellular space. Herewith, the thick-walled vascular structures look more resistant to necrotic destruction compared to thin-walled ones in pristine LLC. This apparently allows LLC + P-MSCs(i.v.) to develop longer than unsupported LLC. Also, a pronounced cellular/nuclear polymorphism is present.

3.3 | P-MSCs promote LLC metastasis to the lungs

The chosen variant of the engrafted carcinoma allows to study not only the primary tumor but also the metastasis process. The lungs of mice in the control intact group have a typical histological structure with normal polygonal shape and thickness of alveolar walls (5–10 μm) as well as uniform alveolar diameter (Figure S20a). The microcirculatory bed (capillaries) is well developed, there are no signs of hyperemia, inflammation or destruction of alveolar walls. The terminal and respiratory bronchioles and alveolar ducts are clean; alveolar macrophages are almost absent in them.

On the 10th day of LLC development, the lung structure is generally normal but with small areas of inflamed fibrosis (1.5% in respect to the whole sample area), single micrometastases, alveolar septa destruction and slight lymphocytic infiltration (Figure 5A and S20b,c). Also, macrophages are increased in number in the terminal and respiratory bronchioles (Figure S20c).

In the LLC + P-MSCs (Figures 5A and S21a) and LLC + P-MSCs (i.v.) models (Figures 5A and S22a), the inflamed fibrous area is ~16% (Figure 5D). The individual single micrometastatic nodes of perivascular and peribronchial localization are noted with the tumor node area of ~8% (Figure 5E) and the total metastasis number of 9 per cm^2 (Figure 5F), where the number of large metastases (Ø ≥ 1 mm) prevails in the LLC + P-MSCs model (3.2 against 1.4 cm^{-2}). Also, more pronounced changes in the histological organization of lung tissue occur: slightly thickened alveolar walls (mainly due to interstitial lymphocytic infiltrate), an increased number of alveolar macrophages in alveoli and an augmented blood supply to microvasculature (Figures S20c, S21a, and S22a). All these signs indicate more active initial phases of the inflammatory process in the lungs, compared to pristine LLC.

In all models on the 15th day, a large morphological diversity of changes is observed in the histological structure of lungs both within the same organ and between different animals: from the preservation of almost normal structure to inflammatory and fibrotic changes as well as formed metastases with necrotic areas (Figure 5B).

In the LLC model, the inflamed fibrous area in the lung tissue is 13% (Figure 5B,D and Figure S20d–h) and the tumor node area is 9% (Figure 5E). The tumor nodes are very small, located along the lung periphery (a usual arrangement of metastasis) and have the form of clearly defined compact nodes (Figure S20e,f); their total number is 19 cm^{-2} (Figure 5F) so that the number and size of micrometastatic nodes are rising (2.4 cm^{-2} of nodes ≥1 mm). The average diameter of

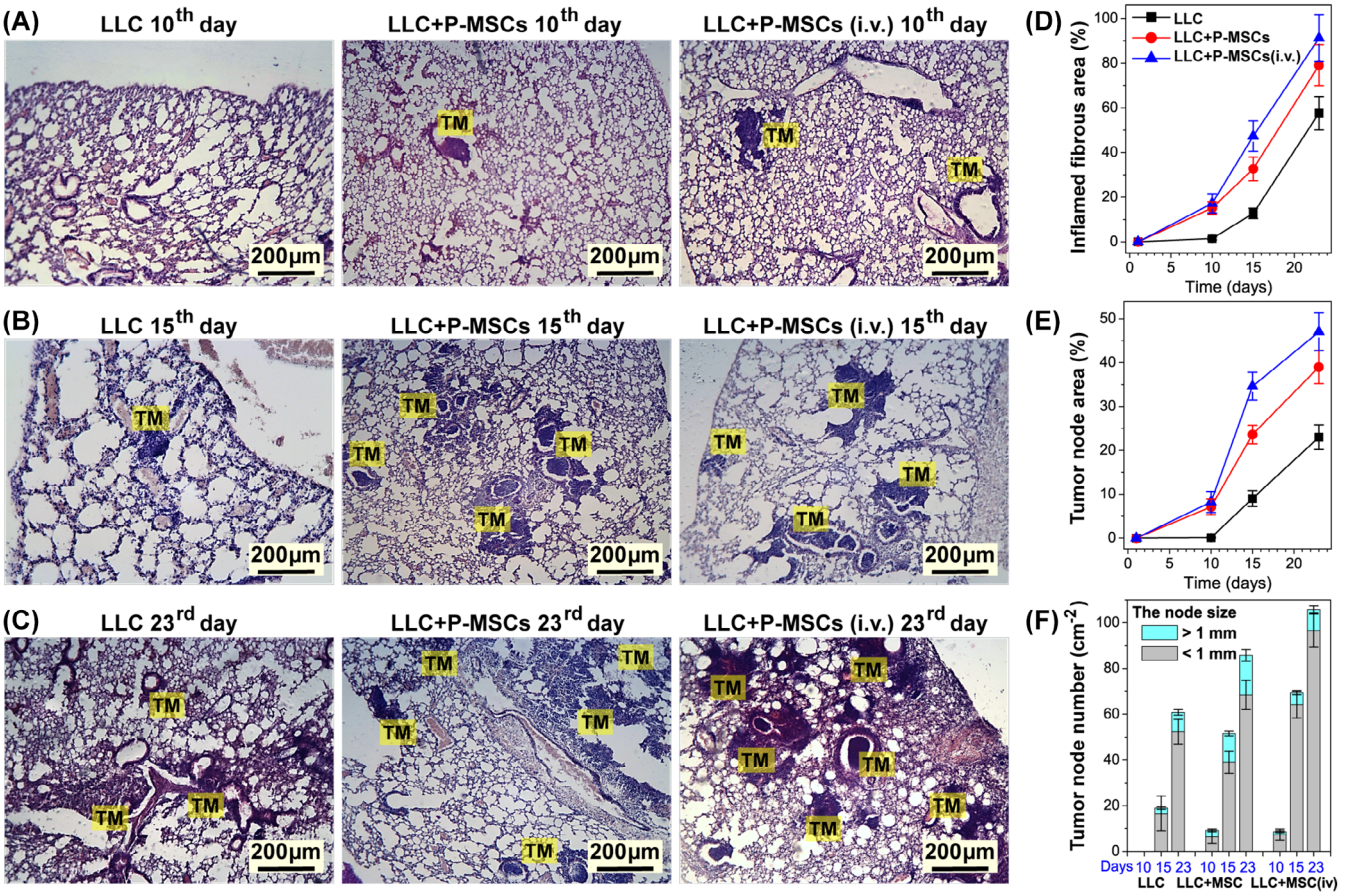

FIGURE 5 Histopathology of the metastasis in the mouse lungs on (A) the 10th, (B) 15th, and (C) 23rd day of LLC, LLC + P-MSCs and LLC + P-MSCs(i.v.) development (TM – tumor metastasis). Graphics of the quantitative morphometric analysis of lung lesions: (D) an inflamed-fibrous area and (E) a tumor node area in respect to the whole sample area, and (F) the metastasis number with two diameter ranges per cm^2. All data are shown as the mean ± SE from each group, $p < 0.05$ for data with a statistically significant difference (two-way ANOVA test). [Color figure can be viewed at wileyonlinelibrary.com]

blood vessels and the area of alveolar ducts are increased by ~25% compared to the normal lungs, which may indicate the initial process of inflammation and invasion of the cancer cells. The lymphocytic infiltration of alveolar septa is increased, especially, in the peribronchiolar areas (lymphocytic hyperplasia) where the tumor cells are detected. In some areas, the blood filling of the capillary bed is increased, which is accompanied by diapedesis of erythrocytes (Figure S20g), their destruction outside vessels and, as a result, an accumulation of siderophages (Figure S20h).

In the LLC + P-MSCs model, the lung has a similar structure as in the LLC model, however, the fibrous area is 35% (Figures 5B,D and S21b,c) and the tumor node area is 24% (Figure 5E). The number and size of diffuse micrometastases are substantially larger (51.6/11.4 cm^{-2} of the ratio of the total to large nodes) than in the LLC group (Figures 5F and S21d,e). So, these parameters are increased by ~2.6 times compared to the LLC model. Also, a noticeably increased lymphocytic infiltration of alveolar septa (Figure S21d) is leading to their complete destruction.

In LLC + P-MSCs(i.v.), the fibrous area is as large as 48% (Figures 5B,D and S22b,c), the tumor node area is 35% (Figure 5E), and the ratio of the total to large nodes is 69.4/5.2 cm^{-2} (Figure 5F). So, the metastasis area and number are exceeding by more than 3 times compared to those in pristine LLC. The third part of mice demonstrates the most preserved variant of the histological structure of lungs, but they also differ from the normal one: thickened alveoli walls, a decreased diameter of alveoli, an expansion of alveolar ducts as well as the presence of the micronodules containing a small number of the cells. In other animals, there are significant expansions of alveolar ducts as a result of the destruction of alveolar walls (Figure S22d), the fibrotic changes in lung parenchyma (with thickened alveolar walls, a diminished lumen and, accordingly, a decreased gas exchange function), interstitial hemorrhages with the release of erythrocyte mass outside vessels (Figure S22d–f). This feature is the pronounced hyperplastic changes in the epithelium of bronchioles (lesions) (Figure S22g). In 33% of animals, the hyperplastic process with the formation of a large accumulation of cells inside the lumen of terminal bronchioles occurs (Figure S22h–j), evidencing a triggered proliferation of their epithelial cells.

On the 23rd day of LLC tumor development, the inflamed fibrous area is 58% (Figure 5D), the tumor node area is 23% (Figure 5E), and the ratio of the total to large nodes is 60.8/8.4 cm^{-2} (Figure 5F). There are signs of inflammation in the lung parenchyma (lymphocytic

infiltration, vasodilation and alveolar hemorrhages), changes in the structure of bronchioles (expansion) and alveoli (change in shape, decrease in diameter and fibrous changes in the walls) and small foci of proliferating cells (mainly peribronchial) (Figures 5C and S20i).

In the LLC + P-MSCs and LLC + P-MSCs(i.v.) models, the listed changes are more pronounced than in LLC (Figures 5C and S22f,k). The fibrosis area (80–90%) is increased by ~1.5 times. The tumor node area (39–47%) is increased by ~2 times. The ratio of the total number of nodes to the number of large nodes is 85.8/17.4 and 105.8/9.2 cm^{-2}, respectively. Therefore, these models favor aggressiveness of metastasis: many small metastatic nodes and diffuse foci of tumor cell accumulation are seen, where the number of large metastases prevails in LLC + P-MSCs.

3.4 | Secretion of angiogenic factors by LLC cells and P-MSCs

The tumor of LLC + P-MSCs on the 15th day lags behind in growth from LLC and LLC + P-MSCs(i.v.), while on the 23rd day, the tumor volume in all the groups did not differ significantly. Tumor growth depends on angiogenesis; the major angiogenic growth factors that promote vascular development are TGF-β, VEGF and IL-6. The secretion of these factors has been assayed (by ELISA kits, according to the manufacturer's protocols by ThermoFisher Scientific, USA) in vitro (Table S2). There is a weak production of TGF-β (180 and 36 pg/mL), VEGF (90 and 27 pg/mL) and IL-6 (120 and 24 pg/mL) in separately cultivated LLC and P-MSCs, respectively. While TGF-β, VEGF and IL-6 secretion by P-MSCs is greatly increased (774, 207, and 372 pg/mL, respectively) when they are incubated in the conditioned medium from LLC, that suggests a strong paracrine effect of LLC on P-MSCs. The stimulating effect of the conditioned medium from P-MSCs on the secretion of the growth factors by LLC cells was less pronounced (216, 99, and 138 pg/mL, respectively). When co-cultivating LLC + P-MSCs (1:1), their production of the growth factors is reduced (126, 45, and 72 pg/mL, respectively) compared to that by the control LLC cells. On the contrary, when co-cultivating LLC + P-MSCs (5:1), the secretion of the growth factors is very high (648, 216, and 468 pg/mL, respectively), being comparable to that by P-MSCs in the conditioned medium from LLC.

3.5 | P-MSCs cause polyploidy of LLC cells

Cancer cells are often characterized by changes in ploidy, being a sign of tumor aggressiveness [33, 34]. The karyotype analysis of tumor cells in the LLC, LLC + P-MSCs and LLC + P-MSCs(i.v) models shows the absence of cell aneuploidy, such as monosomy and trisomy, only in pristine LLC. On the contrary, at the presence of MSCs, LLC cells own complex karyotypes with cell clones having different numbers of chromosomes (cytogenetic characterization in Figure 6). Based on MGI-Rules for Nomenclature of Chromosome Aberrations (informatics.jax.org), the modal number has been determined: the diploid set is 2n = 40; 1n = 20; hyperdiploid – 41–49, hypodiploid – 30–39; hypotriploid – 51–59, hypertriploid – 61–69; hypotetraploid – 71–79, hypertetraploid – 81–89; and so forth.

The results are presented based on the analysis of 30 metaphases for each sample on the 15th day of tumor development, when an active metastasis begins. In LLC (Figure 6A,D), there are a complex hyperdiploid karyotype with 49 chromosomes (46.7% of cells; 14 of 30 analyzed metaphases) and hypotriploid cell lines containing 54 (43.3%; 13/30) and 58 chromosomes (10%; 3/30). In LLC + P-MSCs(i.v.) (Figure 6B,D), there are a hyperdiploid karyotype of 49 (43.3%; 13/30), hypotriploid cell lines of 56 (36.7%; 11/30) and 52 (10%; 3/30) and a hypertriploid one of 64 (10%; 3/30). In LLC + P-MSCs (Figure 6C,D), the cell karyotype is the most complex with heterogeneous chromosomal structure. There are hypotriploid karyotypes of 54 (20%; 6/30), 52/56 (13.3%; 4/30), 53/55 (10%; 3/30), 49/50/51/58 (6.7%; 2/30), 57 (3.3%; 1/30) and a hypotetraploid karyotype of 74 (3.3%; 1/30).

4 | DISCUSSION

The effect of P-MSCs on the primary tumor growth and metastasis in the LLC, LLC + P-MSCs and LLC + P-MSCs(i.v.) models has been comprehensively investigated. Expectably that the resultant distribution of MSCs in the animals, depending on the route of administration, provides a key effect on cancer development. It is known that the most widely used i.v. administration of MSCs leads to the initial accumulation of the cells into the lungs, followed by their redistribution to the liver, spleen and kidneys, as well as, then, throughout the body. Withal, the tendency of MSCs to migrate toward the pathology zone is persisted. At i.m., intraarticular and intradermal administration of MSCs, there is no systemic biodistribution, so, the cells primarily accumulate in an injection zone [35, 36]. Thus, we have assumed that, at the simultaneous i.m. injection of LLC + MSCs, the concentration of MSCs near the muscle tissue was higher than when they were i.v. injected into the tail vein.

These two different injection methods resulted in the opposite direction of tumor development. The LLC + P-MSCs tumor had a smaller size with highly suppressed vascularization than in the control pristine LLC on the 15th day. The deceleration effect of MSCs was observed in many other models [12–20]. The deceleration effect of human MSCs on the proliferation of EC and the reduction of EC vascular network formation was also reported [37]. On the contrary, in LLC + P-MSCs(i.v.), P-MSCs stimulated the growth of the primary tumor and angiogenesis. On the 15th and 23rd days, the LLC + P-MSCs(i.v.) tumor was better supplied with differentiated vessels sprouting from surrounding tissues; on the 15th day, the tumor was already actively developing its own provascular structures. Moreover, the presence of P-MSCs induced tumor neoangiogenesis. Other studies also showed the stimulatory effect of MSCs on the growth of the primary tumors [4–11]. The enhancement of neovascularization has been noted in several studies [6, 9, 10] showing that MSCs directly supported the tumor vasculature by localizing close to vascular walls

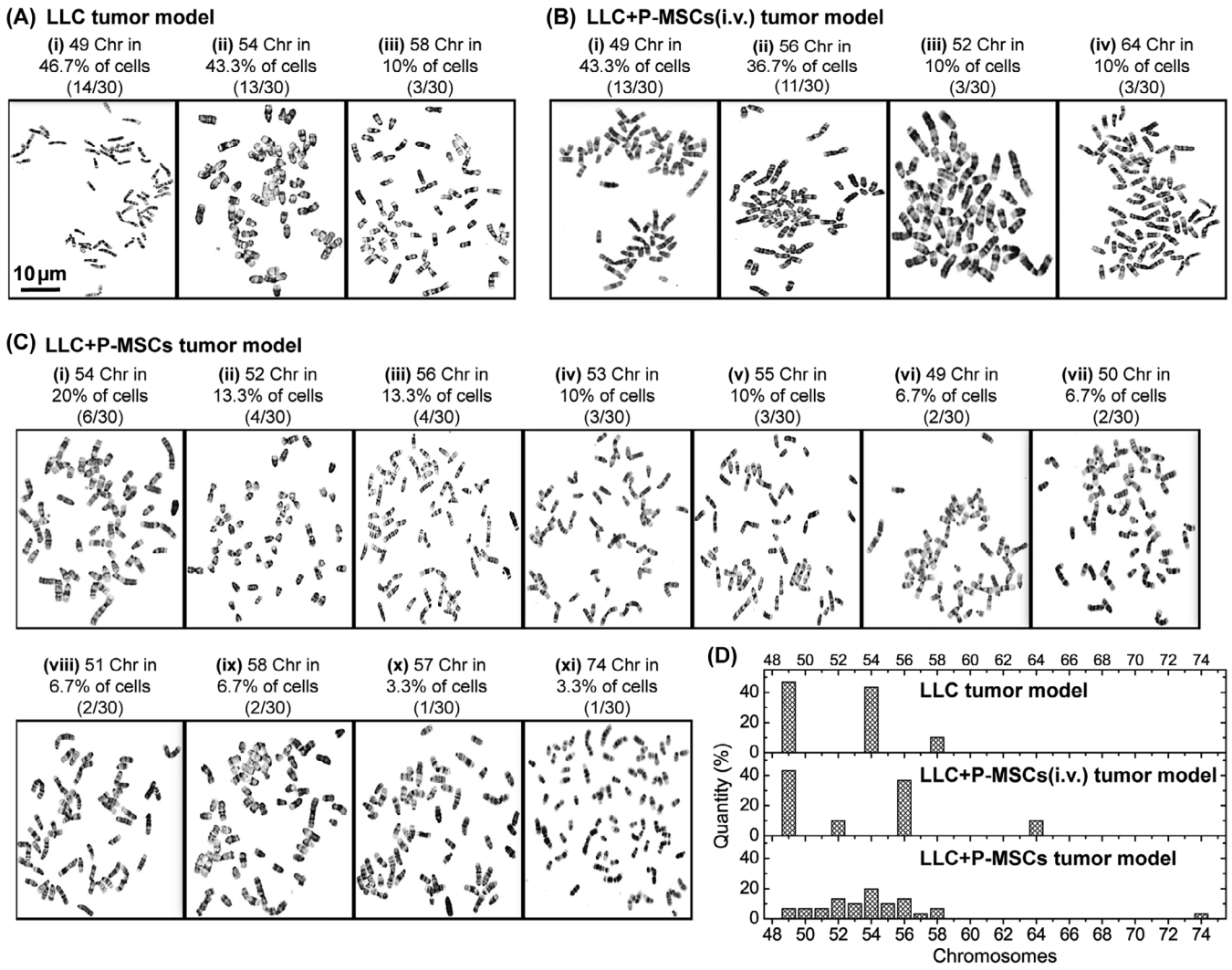

FIGURE 6 Metaphase chromosome plates prepared from the cells of (A) LLC, (B) LLC + P-MSCs, and (C) LLC + P-MSCs(i.v.) tumor models. (D) Quantitative karyotype analysis versus the chromosome modal number.

and by expressing an endothelial marker. The variability of the obtained results, expressed in the pro-tumorigenic or anti-tumorigenic potential of MSCs, can be explained by different types of tumor models or sources of MSCs. Thus, the manifestation of the MSC effect depends on the experimental conditions, which can change the secretion of various factors produced by MSCs [38].

The ability of P-MSCs to secrete the proangiogenic factors TGF-β, VEGF and IL-6 was assessed in vitro, suggesting a robust bidirectional paracrine effect of LLC on P-MSCs: a downregulated secretion when co-cultivating an equal amount of LLC cells and P-MSCs and, in contrast, an upregulated secretion when several cancer cells are contacted to a single P-MSC. In the co-inoculated LLC + P-MSCs tumor group, as at the in vitro co-cultivation of an equal amount of LLC cells and P-MSCs, the secretion of angiogenic growth factors could be downregulated. By this means, a deficiency of sufficient production of TGF-β, VEGF and IL-6 slowed down the angiogenesis and tumor growth compared to the control. On the contrary, in the LLC + MSCs (i.v.) group, the amount of MSCs initially significantly less than that after co-inoculation, because some of MSCs injected into the tail vein were retained in the lungs, liver and other organs [35]. In this case, the LLC tumor response to the arriving P-MSCs was probably similar to that at LLC + P-MSCs co-incubation in vitro at a ratio 5:1, when the secretion of growth factors was significantly upregulated. Thereby, the stimulated primary tumor growth, angiogenesis and metastasis were observed. It is known that VEGF secreted by MSCs promotes differentiation of endothelial progenitor cells into EC through the paracrine mechanisms [39].

Thus, the ability of cancer cells to stimulate the secretion of proangiogenic factors by means of MSCs has been shown, as a result, to accelerate the growth of the primary tumor. Though, this possibility can be realized only when cancer cells dominate. On the contrary, at contact interaction of an equal number of MSCs and cancer cells, the downregulation of growth factor secretion can be observed, that slow down the growth of the primary tumor.

Transplanted LLC has a selectivity for hematogenous lung metastasis. The rate and volume of metastatic lesions are defining indicators

of tumor aggressiveness. We observed that the volume of metastatic lesions in animals with LLC + P-MSCs and LLC + P-MSCs(i.v.) was significantly greater compared to pristine LLC. The metastasis was accompanied by a number of changes in the lung parenchyma, which indicates the development of an inflammatory process: thickening of the alveolar walls, their infiltration with inflammatory cells, initial fibrosis, hemorrhages, expansion of the alveolar ducts and bronchioles. An increased induction of hyperplastic processes in the lung parenchyma, in particular, in the epithelium of terminal bronchioles, had the most pronounced character. At the same time, in LLC + P-MSCs(i.v.), the increase in the metastasis node volume was mainly due to an increase in small metastases, probably, due to the dissemination of single cells via a highly developed vascular system. While, in LLC + P-MSCs, the percentage of large metastases was higher, so, the probability of collective metastasis of tumor cells was increased facilitating introvasion into fewer but more structured vessels.

The more aggressive metastasis in the presence of MSCs can be explained by the increased polyploidy of LLC under the action of MSCs. Ploidy disorders may cause chromosomal instability (CIN), which contributes to the loss of heterozygosity (LOH) [33, 34]. LOH is a common change in cancer development that results in the loss of gene expression and often affects tumor suppressor genes, thereby promoting tumorigenesis. CIN and subsequent possible polyploidy-induced LOH, alone or together with other genetic or epigenetic changes, may affect the ability of cancer cells to migrate and invade [40–42].

Summing up, these findings indicate a multidirectional effect of human P-MSCs on the growth of LLC in the early periods after injection, depending on the injection method and the number of contacting cells. In the long term after injection, the effect of MSCs on the growth of the primary tumor is not manifested. At the same time, regardless of the injection method, P-MSCs increase LLC aggressiveness related to cancer-associated angiogenesis and metastasis activation. It is important to note here that the introduction of MSCs to the control healthy animals without tumors did not stimulate any pathology. This sure indicates the possibility of using MSCs in regenerative therapy and for diagnostic purposes. However, its potential stimulation of cancer aggressiveness should be considered for safer use of MSCs in case of inadequately examined patients or a possible undefined tumor at its early stages. Yet, the limitations of the current research are related to the use of human P-MSCs to influence cancerous environment in an animal. It is worth noting that the results could be somewhat different if other MSCs would be used, because of specific levels of secreted pro- or antitumorigenic and proangiogenic factors.

5 | CONCLUSIONS

The direction of influence of human P-MSCs on the LLC tumor development and metastatic potential has been investigated. The action of P-MSCs can possess both pro-tumorigenic and anti-tumorigenic potential depending on the injection method. After intramuscular co-inoculation of LLC and P-MSCs (LLC + P-MSCs), the growth of the primary tumor and angiogenesis are slowed down compared to the control LLC on the 15th day. This has been explained by the fact of a decrease in the secretion of proangiogenic factors during in vitro co-cultivation of an equal amount of LLC cells and P-MSCs. On the contrary, when P-MSCs are intravenously (i.v.) injected in the mice with developing LLC (LLC + P-MSCs(i.v.)), the tumor growth and angiogenesis are stimulated on the 15th day. A highly activated secretion of proangiogenic factors by P-MSCs in a similar in vitro model can explain this. In both the models compared to the control on the 23rd day, there is no significant difference in the tumor growth, while angiogenesis remains correspondingly decelerated or stimulated. At the same time, P-MSCs contribute to the activation of metastasis, regardless of the injection model. The total volume and number of lung metastases constantly increase compared to the control: it is mainly due to small-size metastases for LLC + P-MSCs(i.v.), while the fraction of large metastases increases for LLC + P-MSCs. The stimulation of metastasis might be dependent on the constantly increased angiogenesis activity. The increase in the rate of LLC cell dissemination after the P-MSCs injection is explained by the disordered polyploidy and CIN, which can lead to an increase in migration and invasion of cancer cells. The more aggressive metastasis in the presence of MSCs can be explained by the fact that, after LLC + P-MSCs co-inoculation, the tumor cell karyotype has the most complex and heterogeneous chromosomal structure.

AUTHOR CONTRIBUTIONS

Iuliia Golovynska: Conceptualization; investigation; funding acquisition; writing – original draft; methodology; visualization; writing – review and editing; validation; software. **Yurii V. Stepanov:** Conceptualization; investigation; writing – original draft; methodology; data curation; validation; formal analysis. **Galyna Ostrovska:** Investigation; methodology; validation. **Larysa Pylyp:** Investigation; methodology. **Taisa Dovbynchuk:** Investigation; methodology. **Liudmyla I. Stepanova:** Investigation; methodology. **Oleksandr Gorbach:** Investigation; methodology; software. **Volodymyr Shablii:** Investigation; methodology; software. **Hao Xu:** Investigation; methodology. **Liudmyla V. Garmanchuk:** Funding acquisition; project administration; data curation; supervision; resources. **Tymish Y. Ohulchanskyy:** Funding acquisition; project administration; resources; supervision; data curation. **Junle Qu:** Funding acquisition; project administration; resources; supervision; data curation. **Galina I. Solyanik:** Methodology; validation; formal analysis; project administration; data curation; supervision; resources.

FUNDING INFORMATION

This work has been partially supported by the National Key R&D Program of China (2021YFF0502900); National Natural Science Foundation of China (61835009/62127819); Shenzhen Key Laboratory of Photonics and Biophotonics (ZDSYS20210623092006020) and Shenzhen Science and Technology Program (JCYJ20220818100202005) and National Academy of Sciences of Ukraine (2.2.5.443).

CONFLICT OF INTEREST STATEMENT

The authors declare no conflicts of interest.

PEER REVIEW

The peer review history for this article is available at https://www.webofscience.com/api/gateway/wos/peer-review/10.1002/cyto.a.24814.

DATA AVAILABILITY STATEMENT

The datasets used and/or analyzed during the current study are available from the corresponding author on reasonable request.

ORCID

Yurii V. Stepanov https://orcid.org/0000-0002-6349-631X
Iuliia Golovynska https://orcid.org/0000-0003-3916-6588
Galyna Ostrovska https://orcid.org/0000-0002-3307-9099
Larysa Pylyp https://orcid.org/0000-0003-0039-7557
Taisa Dovbynchuk https://orcid.org/0000-0001-7451-6315
Liudmyla I. Stepanova https://orcid.org/0000-0002-8833-9409
Volodymyr Shablii https://orcid.org/0000-0002-1058-7947
Hao Xu https://orcid.org/0000-0002-4447-7746
Liudmyla V. Garmanchuk https://orcid.org/0000-0002-1527-2346
Tymish Y. Ohulchanskyy https://orcid.org/0000-0002-7051-6534
Junle Qu https://orcid.org/0000-0001-7833-4711
Galina I. Solyanik https://orcid.org/0000-0002-8657-1263

REFERENCES

1. Studeny M, Marini FC, Dembinski JL, Zompetta C, Cabreira-Hansen M, Bekele BN, et al. Mesenchymal stem cells: potential precursors for tumor stroma and targeted-delivery vehicles for anticancer agents. J Natl Cancer Inst. 2004;96(21):1593–603.
2. Klopp AH, Spaeth EL, Dembinski JL, Woodward WA, Munshi A, Meyn RE, et al. Tumor irradiation increases the recruitment of circulating mesenchymal stem cells into the tumor microenvironment. Cancer Res. 2007;67(24):11687–95.
3. Sun Z, Wang S, Zhao R. The roles of mesenchymal stem cells in tumor inflammatory microenvironment. J Hematol Oncol. 2014;7(1):14.
4. Zhu W, Xu W, Jiang R, Qian H, Chen M, Hu J, et al. Mesenchymal stem cells derived from bone marrow favor tumor cell growth in vivo. Exp Mol Pathol. 2006;80(3):267–74.
5. Karnoub AE, Dash AB, Vo AP, Sullivan A, Brooks MW, Bell GW, et al. Mesenchymal stem cells within tumour stroma promote breast cancer metastasis. Nature. 2007;449(7162):557–63.
6. Spaeth EL, Dembinski JL, Sasser AK, Watson K, Klopp A, Hall B, et al. Mesenchymal stem cell transition to tumor-associated fibroblasts contributes to fibrovascular network expansion and tumor progression. PloS One. 2009;4(4):e4992.
7. Okumura T, Wang SSW, Takaishi S, Tu SP, Ng V, E Ericksen R, et al. Identification of a bone marrow-derived mesenchymal progenitor cell subset that can contribute to the gastric epithelium. Lab Invest. 2009;89(12):1410–22.
8. Lis R, Touboul C, Mirshahi P, Ali F, Mathew S, Nolan DJ, et al. Tumor associated mesenchymal stem cells protects ovarian cancer cells from hyperthermia through CXCL12. Int J Cancer. 2011;128(3):715–25.
9. Suzuki K, Sun R, Origuchi M, Kanehira M, Takahata T, Itoh J, et al. Mesenchymal stromal cells promote tumor growth through the enhancement of neovascularization. Mol Med. 2011;17(7–8):579–87.
10. Zhang T, Lee YW, Rui YF, Cheng TY, Jiang XH, Li G. Bone marrow-derived mesenchymal stem cells promote growth and angiogenesis of breast and prostate tumors. Stem Cell Res Ther. 2013;4(3):70.
11. Melzer C, von der Ohe J, Hass R. Enhanced metastatic capacity of breast cancer cells after interaction and hybrid formation with mesenchymal stroma/stem cells (MSC). Cell Commun Signal. 2018;16(1):2.
12. Khakoo AY, Pati S, Anderson SA, Reid W, Elshal MF, Rovira II, et al. Human mesenchymal stem cells exert potent antitumorigenic effects in a model of Kaposi's sarcoma. J Exp Med. 2006;203(5):1235–47.
13. Qiao L, Xu Z, Zhao T, Zhao Z, Shi M, Zhao RC, et al. Suppression of tumorigenesis by human mesenchymal stem cells in a hepatoma model. Cell Res. 2008;18(4):500–7.
14. Qiao L, Xu ZL, Zhao TJ, Ye LH, Zhang XD. Dkk-1 secreted by mesenchymal stem cells inhibits growth of breast cancer cells via depression of Wnt signalling. Cancer Lett. 2008;269(1):67–77.
15. Cousin B, Ravet E, Poglio S, De Toni F, Bertuzzi M, Lulka H, et al. Adult stromal cells derived from human adipose tissue provoke pancreatic cancer cell death both in vitro and in vivo. PLoS One. 2009;4(7):e6278.
16. Sun B, Roh KH, Park JR, Lee SR, Park SB, Jung JW, et al. Therapeutic potential of mesenchymal stromal cells in a mouse breast cancer metastasis model. Cytotherapy. 2009;11(3):289–98.
17. Kidd S, Caldwell L, Dietrich M, Samudio I, Spaeth EL, Watson K, et al. Mesenchymal stromal cells alone or expressing interferon-β suppress pancreatic tumors in vivo, an effect countered by anti-inflammatory treatment. Cytotherapy. 2010;12(5):615–25.
18. Li L, Tian H, Chen Z, Yue W, Li S, Li W. Inhibition of lung cancer cell proliferation mediated by human mesenchymal stem cells. Acta Biochim Biophys Sin. 2010;43(2):143–8.
19. Chao K-C, Yang H-T, Chen M-W. Human umbilical cord mesenchymal stem cells suppress breast cancer tumourigenesis through direct cell-cell contact and internalization. J Cell Mol Med. 2012;16(8):1803–15.
20. Lu Y-R, Yuan Y, Wang XJ, Wei LL, Chen YN, Cong C, et al. The growth inhibitory effect of mesenchymal stem cells on tumor cells in vitro and in vivo. Cancer Biol Ther. 2014;7(2):245–51.
21. Noël D, Djouad F, Bouffi C, Mrugala D, Jorgensen C. Multipotent mesenchymal stromal cells and immune tolerance. Leuk Lymphoma. 2009;48(7):1283–9.
22. Bergmann C, Strauss L, Zeidler R, Lang S, Whiteside TL. Expansion of human T regulatory type 1 cells in the microenvironment of cyclooxygenase 2 overexpressing head and neck squamous cell carcinoma. Cancer Res. 2007;67(18):8865–73.
23. Strauss L, Bergmann C, Szczepanski M, Gooding W, Johnson JT, Whiteside TL. A unique subset of CD4+CD25highFoxp3+ T cells secreting interleukin-10 and transforming growth factor-1 mediates suppression in the tumor microenvironment. Clin Cancer Res. 2007;13(15):4345–54.
24. Honczarenko M, le Y, Swierkowski M, Ghiran I, Glodek AM, Silberstein LE. Human bone marrow stromal cells express a distinct set of biologically functional chemokine receptors. Stem Cells. 2006;24(4):1030–41.
25. Khaki M, Salmanian AH, Abtahi H, Ganji A, Mosayebi G. Mesenchymal stem cells differentiate to endothelial cells using recombinant vascular endothelial growth factor-A. Rep Biochem Mol Biol. 2018;6(2):144–50.
26. Mohr A, Zwacka R. The future of mesenchymal stem cell-based therapeutic approaches for cancer – from cells to ghosts. Cancer Lett. 2018;414:239–49.
27. Schweizer MT, Wang H, Bivalacqua TJ, Partin AW, Lim SJ, Chapman C, et al. A phase I study to assess the safety and cancer-homing ability of allogeneic bone marrow-derived mesenchymal stem cells in men with localized prostate cancer. Stem Cells Transl Med. 2019;8(5):441–9.
28. Niess H, von Einem JC, Thomas MN, Michl M, Angele MK, Huss R, et al. Treatment of advanced gastrointestinal tumors with genetically modified autologous mesenchymal stromal cells (TREAT-ME1): study protocol of a phase I/II clinical trial. BMC Cancer. 2015;15(1):237.

29. Hmadcha A, Martin-Montalvo A, Gauthier BR, Soria B, Capilla-Gonzalez V. Therapeutic potential of mesenchymal stem cells for cancer therapy. Front Bioeng Biotechnol. 2020;8:1–13.
30. Ryu H, Oh JE, Rhee KJ, Baik SK, Kim J, Kang SJ, et al. Adipose tissue-derived mesenchymal stem cells cultured at high density express IFN-β and suppress the growth of MCF-7 human breast cancer cells. Cancer Lett. 2014;352(2):220–7.
31. Talwadekar MD, Kale VP, Limaye LS. Placenta-derived mesenchymal stem cells possess better immunoregulatory properties compared to their cord-derived counterparts–a paired sample study. Sci Rep. 2015;5(1):1–12.
32. Moonshi SS, Adelnia H, Wu Y, Ta HT. Placenta-derived mesenchymal stem cells for treatment of diseases: a clinically relevant source. Adv Ther. 2022;5(10):2200054.
33. Couto SS. The pathologist's slide reveals more than meets the eye: loss of heterozygosity and cancer biology. Vet Pathol. 2010;48(1):236–44.
34. Novikov NM, Zolotaryova SY, Gautreau AM, Denisov EV. Mutational drivers of cancer cell migration and invasion. Br J Cancer. 2020;124(1):102–14.
35. Kidd S, Spaeth E, Dembinski JL, Dietrich M, Watson K, Klopp A, et al. Direct evidence of mesenchymal stem cell tropism for tumor and wounding microenvironments using in vivo bioluminescent imaging. Stem Cells. 2009;27(10):2614–23.
36. Sanchez-Diaz M, Quiñones-Vico MI, Sanabria de la Torre R, Montero-Vílchez T, Sierra-Sánchez A, Molina-Leyva A, et al. Biodistribution of mesenchymal stromal cells after administration in animal models and humans: a systematic review. J Clin Med. 2021;10(13):2925.
37. Menge T, Gerber M, Wataha K, Reid W, Guha S, Cox CS Jr, et al. Human mesenchymal stem cells inhibit endothelial proliferation and angiogenesis via cell–cell contact through modulation of the VE-cadherin/β-catenin signaling pathway. Stem Cells Dev. 2013;22(1):148–57.
38. Klopp AH, Gupta A, Spaeth E, Andreeff M, Marini F III. Concise review: dissecting a discrepancy in the literature: do mesenchymal stem cells support or suppress tumor growth? Stem Cells. 2011;29(1):11–9.
39. Ge Q, Zhang H, Hou J, Wan L, Cheng W, Wang X, et al. VEGF secreted by mesenchymal stem cells mediates the differentiation of endothelial progenitor cells into endothelial cells via paracrine mechanisms. Mol Med Rep. 2017;17(1):1667–75.
40. Healy KD, Hodgson L, Kim TY, Shutes A, Maddileti S, Juliano RL, et al. DLC-1 suppresses non-small cell lung cancer growth and invasion by RhoGAP-dependent and independent mechanisms. Mol Carcinog. 2008;47(5):326–37.
41. Heering J, Erlmann P, Olayioye MA. Simultaneous loss of the DLC1 and PTEN tumor suppressors enhances breast cancer cell migration. Exp Cell Res. 2009;315(15):2505–14.
42. Tripathi V, Popescu NC, Zimonjic DB. DLC1 induces expression of E-cadherin in prostate cancer cells through Rho pathway and suppresses invasion. Oncogene. 2013;33(6):724–33.

SUPPORTING INFORMATION

Additional supporting information can be found online in the Supporting Information section at the end of this article.

How to cite this article: Stepanov YV, Golovynska I, Ostrovska G, Pylyp L, Dovbynchuk T, Stepanova LI, et al. Human mesenchymal stem cells increase LLC metastasis and stimulate or decelerate tumor development depending on injection method and cell amount. Cytometry. 2024;105(4):252–65. https://doi.org/10.1002/cyto.a.24814